Hindawi
Geofluids
Volume 2022, Article ID 2932850, 11 pages
https://doi.org/10.1155/2022/2932850

Research Article

A Calculation Method for Ground Shock Effect Induced by Hypervelocity Impact

Junnan Zhang,[1] Derong Wang,[1] Tianhan Xu,[1] Jie Li,[1] Zhen Wang,[2] Yuguo Ji,[2] and Xiaohui Xu[1]

[1]*State Key Laboratory of Explosion & Impact and Disaster Prevention & Mitigation, Army Engineering University of PLA, Nanjing 210007, China*
[2]*School of Mechanical Engineering, Nanjing University of Science and Technology, Nanjing 210094, China*

Correspondence should be addressed to Derong Wang; wdrjb@163.com and Tianhan Xu; martinxu41@126.com

Received 15 April 2022; Accepted 27 June 2022; Published 11 July 2022

Academic Editor: Dongjiang Pan

In the hypervelocity impact event, the strong ground shock effect is induced and may cause damage to underground engineering. The existing experimental methods and calculation procedures have difficulties in estimating the ground shock under complicated and large-scale impacts. Analytical and experiential methods independently prove that the shock energy radiating from a certain region underground is proportional to the mass of the materials in the region. Based on this relationship, an equivalent method is proposed to estimate the impact-induced ground shock with the help of abundant research results for underground explosions: The ground shock of two events can be seen as being equivalent as long as their crater sizes are the same. The calculated ground shock effect is compared with the measured values in impact experiments, and the results show great agreement.

1. Introduction

Hypervelocity impact on geomaterials can induce strong shock waves, namely ground shock, propagating deeply into the earth and cause damage to underground engineering. The surrounding rocks of the engineering will be unstable under the disturbance of ground shock. It is of necessity and interest to evaluate the characteristics of ground shock produced by a meteorite impact or a kinetic weapon strike.

The most direct method to determine the profiles of impact-induced ground shock is to measure them with gauges in experiments. This is usually done in laboratories with scale models. Nakazawa [1] conducted impact experiments with copper impactors and basalt targets. The gauges were sandwiched between adjacent target plates to measure shock pressure at different distances away from the impact center. Shirai et al. [2] investigated the shock pressure and attenuation in water ice with the impact velocities between 3.9 and 4.6 km/s. Wang et al. [3] impacted granite targets with steel projectiles and measured shock pressure with in-material gauges. On the other hand, theoretical investigations on the evolution of impact-induced ground shock were also carried out by some researchers, such as Melosh [4] and Mok [5]. These investigations are usually based on Hugoniot equations.

The aforementioned studies can well obtain and predict the ground shock induced by relatively simple and small-scale impacts but may lack simplicity and accuracy for complex and large-scale impacts. Besides, for impacts that already happened, e.g., historical meteorite impacts, traditional methods lose validity to determine the ground shock experienced. For this case, investigations are mainly carried out using observation methods [6–8]. However, crater observations also showed some uncertainty when quantitative analysis is required.

A convenient and steady method for estimating ground shock is thus necessary. From the aspect of energy and work and considering the fact that the essence of ground shock is the motion of material particles and grains, the energy of ground shock originates from the work done by the force expanding the crater. In this connection, it is possible to build a relationship between the crater and the ground shock in terms of energy. On the other hand, given that the shallow-buried explosion and hypervelocity impact are similar in crater shape and that the scale of experimental data of explosion-induced ground shock is much larger, it will be of practical significance if the equivalent transformation from hypervelocity impact to shallow-buried explosion can be established. This paper attempts to realize these ideas and to provide a convenient calculation procedure for reviewing and predicting the impact-induced ground shock.

2. Characteristic Energy Factor of Ground Shock

In the center of the action, forces on the free surface push rock materials outward to form a cavity. Meanwhile, a proportion of the total energy is transmitted into rock masses in the form of shock waves through doing work. In the vicinity of the cavity, the damage region occurs due to shock pressure larger than the rock strength.

A confined explosion can be seen as being in an infinite and isotropic medium. As is shown in Figure 1, a spherical cavity with radius r_0 is formed in the explosion center. The damage region adjacent to the cavity can be roughly divided into two parts, i.e., a fracture region with radius r_f and a radial-crack region with radius r_c [9]. Beyond the damage region, rocks deform elastically. The dissipation of the shock energy occurs during the process of propagation, and only approximately 5% of the total explosion energy remains when ground shock propagates across the surface of the damage region, S_c [10]. This part is also known as seismic waves.

After the detonation, the rocks expand outward symmetrically. The motion of rocks can be described in a spherical coordinate system with the charge as the origin. The energy of the ground shock radiating from a certain spherical surface with radius r can be expressed as the work done by shock stress:

$$W = S_r \int_0^{u_r(\infty)} \sigma_r du_r = S_r \int_0^{\infty} \sigma_r \frac{\partial u_r}{\partial t} dt. \tag{1}$$

where σ_r is the radial stress, u_r is the radial displacement, $u_r(\infty)$ is the residual displacement when $t \longrightarrow \infty$, $S_r = 4\pi r^2$ is the surface area of the sphere with radius r, and t is the time.

The evolution of displacement of rocks in the damage region is difficult to calculate due to its complicated mechanism. However, the displacement in the elastic region can be described by the potential function of the form

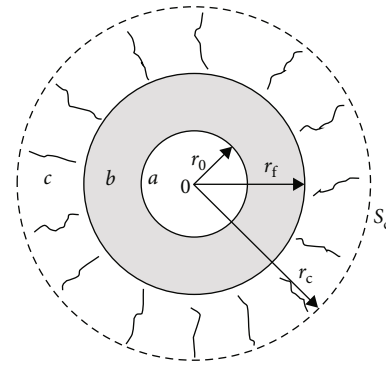

Figure 1: Diagram of the damage region in a confined explosion: (a) cavity; (b) fracture region; (c) radial-crack region.

$$u_r(t, r) = \frac{\partial \varphi(t, r)}{\partial r}, \tag{2}$$

where the potential function $\varphi(t, r)$ is given by Haskell [11], i.e.

$$\begin{aligned} \varphi(t, r) &= -\frac{\psi}{r} f(\tau), \\ \tau &= \frac{1}{t_0}\left(t - \frac{r}{C_p}\right), \\ f(\tau) &= 1 - e^{-\tau}\left(1 + \tau + \frac{\tau^2}{2} + \frac{\tau^3}{6} - B\tau^4\right), \end{aligned} \tag{3}$$

where C_p is the propagation velocity of longitudinal waves, $t_0 \approx r_c/C_p$ is the characteristic time of the shock motion, and ψ and B are unknown parameters. In the elastic model, $B \approx \nu$, where ν is the Poisson's ratio.

The displacement and stress fields of the elastic region are derived from Equations (2) and (3) [12]:

$$\begin{aligned} \frac{u_r}{C_p t_0} &= \lambda_* \left(\frac{f(\tau)}{R^2} + \frac{f'(\tau)}{R}\right), \\ \frac{\sigma_r}{\rho C_p^2} &= -\lambda_* \left(4\gamma^2 \frac{f(\tau)}{R^3} + 4\gamma^2 \frac{f'(\tau)}{R^2} + \frac{f''(\tau)}{R}\right), \\ \frac{\sigma_\theta}{\rho C_p^2} &= \lambda_* \left[2\gamma^2 \frac{f(\tau)}{R^3} + 2\gamma^2 \frac{f'(\tau)}{R^2} - \left(1 - 2\gamma^2\right)\frac{f''(\tau)}{R}\right], \\ \frac{\sigma_r - \sigma_\theta}{2\rho C_p^2} &= -\lambda_* \left(3\gamma^2 \frac{f(\tau)}{R^3} + 3\gamma^2 \frac{f'(\tau)}{R^2} + \gamma^2 \frac{f''(\tau)}{R}\right), \end{aligned} \tag{4}$$

where σ_θ is the circumferential stress, ρ is the density of rocks, $R = r/(C_p t_0)$, $\gamma = C_s/C_p$, C_s is the shear-wave velocity,

and

$$\lambda_* = \frac{\psi}{\left(C_p t_0\right)^3}. \tag{5}$$

The residual displacement and stress follow from Equation (4) as $t \longrightarrow \infty$:

$$\begin{aligned} \frac{u_r(\infty)}{C_p t_0} &= \frac{\lambda_*}{R^2}, \\ \frac{\sigma_r(\infty)}{\rho C_p^2} &= -\frac{4\gamma^2\lambda_*}{R^3}, \\ \frac{\sigma_\theta(\infty)}{\rho C_p^2} &= \frac{2\gamma^2\lambda_*}{R^3}, \\ \frac{\sigma_r(\infty) - \sigma_\theta(\infty)}{2\rho C_p^2} &= -\frac{3\gamma^2\lambda_*}{R^3}. \end{aligned} \tag{6}$$

Substituting Equations (4)–(6) into Equation (1) yields the expression of the radiated energy, which consists of two terms, i.e., the elastic potential energy and the ground shock energy. The ground shock energy can be written as

$$W = \frac{\alpha}{4}\lambda_* \rho C_p^2 S_r u_r(\infty), \tag{7}$$

where $\alpha = [5 + 3(1 + 24B)^2]/64$.

Equation (7) describes the ground shock energy radiating from the spherical surface with radius r in the elastic region. Assume that the Tresca criterion is satisfied on the boundary of the elastic region, $r = r_c$, i.e.

$$\sigma_\theta(\infty) - \sigma_r(\infty) = 2\sigma_s, \tag{8}$$

where σ_s is the shear strength of rocks.

Substituting Equations (6) and (8) into Equation (7), the seismic energy radiating from the boundary of the elastic region can be written as

$$W = \frac{\alpha}{12\gamma^2}\sigma_s S_c u_r(\infty), \tag{9}$$

where $S_c = 4\pi r_c^2$. The product $S_c u_r(\infty)$ is the volume being displaced due to forces on the boundary.

Set $r = r_c$ in Equation (6), then

$$u_r(\infty) = \frac{\sigma_s}{3\mu} r_c, \tag{10}$$

where $\mu = \rho C_s^2$ is the shear modulus of rocks. Then the seismic energy can be written as

$$W = \frac{\alpha}{12\gamma^2}\frac{\sigma_s^2}{\mu}\frac{4}{3}\pi r_c^3 = \frac{\alpha}{12\gamma^2}\frac{\sigma_s^2}{\mu} V_c. \tag{11}$$

Equation (11) shows that the seismic energy is proportional to the volume of the entire damage region and the coefficient is only related to the properties of the emplacement rocks.

The damage region can be seen as a hypocenter. For the sake of generality, a dimensionless factor is introduced to describe the energy characteristic of the hypocenter:

$$k = \frac{W}{M_c C_p^2} = \frac{\alpha}{12}\left(\frac{\sigma_s}{\mu}\right)^2, \tag{12}$$

where $M_c = \rho V_c$ is the mass of the hypocenter. The fraction σ_s/μ is the limit shear strain of rocks.

It is obvious that the energy factor k is only determined by the properties of rocks which are easy to measure by laboratorial test. In this connection, a relationship between the seismic energy and the volume (namely mass) of the damage region has been established.

In the case of a shallow-buried explosion. The typical damage region of a shallow-buried explosion is shown in Figure 2. The buried depth of charge is h_b. A crater with radius r_a on the surface is formed. Assume that the boundary of the damage region has a parabolic shape. The maximum depth of the damage region is z_c, and the extent of the damage region along the free surface is assumed to be equal to the diameter of the crater [12]. The falling debris forms an inner ejecta blanket at the bottom of the crater, making the crater depth seems to be shallower.

Introduce a cylindrical coordinate system (r, θ, z) with the r-axis directed along the surface and the z-axis directed downward. The origin is placed at ground zero. The motion of the rocks does not depend on the coordinate θ due to the rotational symmetry. Then the equation of the boundary of the damage region is

$$z = -\frac{z_c}{r_a^2}\left(r^2 - r_a^2\right). \tag{13}$$

The surface area and the volume of the damage region are

$$\begin{aligned} S_c &= 2\pi\int_0^{z_c}\sqrt{r_a^2 - z\frac{r_a^2}{z_c}}dz = \frac{4}{3}\pi r_a z_c, \\ V_c &= \pi\int_0^{z_c}\left(r_a^2 - z\frac{r_a^2}{z_c}\right)dz = \frac{1}{2}\pi r_a^2 z_c. \end{aligned} \tag{14}$$

Equations (9) and (10) apply for the case of the shallow-buried explosion, provided that the radius r_c is replaced by the equivalent hemispheroid radius [12]. For S_c in Equation (14), the equivalent radius $\bar{r}_c$ is such that

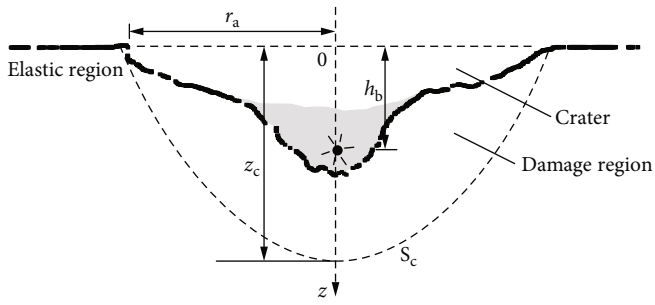

Figure 2: Diagram of the damage region in a shallow-buried explosion.

$S_c = 4\pi r_a z_c/3 = 2\pi \bar{r}_c^{\,2}$, then

$$\bar{r}_c = \sqrt{\frac{2}{3} r_a z_c},$$
$$u_r(\infty) = \frac{\sigma_s}{3\mu}\sqrt{\frac{2}{3} r_a z_c}. \tag{15}$$

Substituting Equations (14) and (15) into Equation (9) yields

$$W = \frac{\sqrt{6}\alpha}{81\gamma^2}\pi\frac{\sigma_s^2}{\mu}(r_a z_c)^{3/2} = \frac{\alpha}{12\gamma^2}\frac{\sigma_s^2}{\mu}V_{c*}, \tag{16}$$

where $V_{c*} = 2\pi\bar{r}_c^{\,3}/3$. Then the energy factor for seismic energy of shallow-buried explosions is

$$k = \frac{W}{M_{c*}C_p^2} = \frac{W}{\rho V_{c*}C_p^2} = \frac{\alpha}{12}\left(\frac{\sigma_s}{\mu}\right)^2. \tag{17}$$

Equation (17) is exactly the same as Equation (12), indicating that the seismic energy factor is a constant for different types of underground explosions with different shapes of damage regions, as long as the rock mass properties are the same. For rocks with $\nu = 0.2 - 0.3$ and $\sigma_s/\mu = (1-2)\times 10^{-3}$, $k = (1.38 - 10.77)\times 10^{-7}$.

Different from the elastic region, the physical and mechanical properties of the cavity and the damage region are too complicated to obtain the analytical solutions for displacement and stress fields. However, the size of each region can be calculated according to its boundary conditions. For confined explosions, for example, [13],

$$r_0 = \frac{\beta Q^{1/3}}{\left(\rho C_p^2\sigma_c^2\right)^{1/9}},$$
$$r_f = r_0\left(\frac{E}{3\sigma_c}\right)^{1/3}, \tag{18}$$
$$r_c = r_f\left(\frac{\sigma_c}{2\sigma_t}\right)^{1/2},$$

where Q is the TNT equivalent of the charge, E is Young's modulus of rocks, $\beta = 9.8\times 10^3$ is the coefficient, and σ_c and σ_t are, respectively, the compressive and tensile strength of rocks.

It is obvious that the ratios between sizes of different regions only depend on the properties of the rocks. On the other hand, it is experimentally proved that the ratios of energy radiating from different boundaries to the charge energy are also constants [10]. In this connection, Wang and Li [13] derived the formulas for the energy factors separately corresponding to the boundaries of the cavity, the fracture region, and the radial-crack region, and the results indicate that they are constants dependent on the properties of rocks. For rocks with $\nu = 0.2 - 0.3$ and $\sigma_s/\mu = (1-2)\times 10^{-3}$, the orders of magnitude of the energy factors are listed in Table 1.

The experiential energy factor of the radical-crack region in Table 1 is consistent with the analytical value calculated with Equation (17), indicating the accuracy and stability of the energy factor. In this connection, it is reliable to estimate the energy radiating from a certain region with its mass or volume. It is noteworthy that the aforementioned calculation procedure is valid for explosions as well as impacts: On the one hand, the form of the potential function $\varphi(t, r)$ is independent from the type of the initial action; on the other hand, the size of each region is determined by its boundary conditions, which are related to the rock strength and also have nothing to do with the type of the action.

3. The Ground Shock of Shallow-Buried Explosions

The last section proves theoretically that the energy of ground shock depends on the extent of the damage region. In practice, it is more convenient to describe the characteristics of explosions in terms of the TNT equivalent of the charge. In this connection, the relationship between the charge and the crater size should be given.

An empirical relationship is given by Henrych [14] using the law of conservation of energy, i.e.,

$$Q = \left(A_1 h_b^3 + A_2 h_b^4 + A_3 h_b^2\right) f(\omega), \tag{19}$$

Table 1: Orders of magnitude of the energy factors of different regions.

Regions	k
Cavity	10^{-3}
Fracture region	10^{-5}
Radial-crack region	10^{-7}

where A_i $(i = 1, 2, 3)$ are coefficients determined by experiments, $\omega = r_a/h_b$ is the parameter describing the geometry of the crater, and $f(\omega)$ is a function of ω which satisfies $f(1) = 1$.

The terms with h_b^3, h_b^4, and h_b^2 correspond to the kinetic energy, the gravitational potential energy, and the surface energy of the ejected rocks, respectively.

For a wide range of ω, e.g., $0.7 \le \omega \le 20$, $f(\omega)$ can be written as [14]

$$f(\omega) = \left[\frac{1+\omega^2}{2}\right]^2. \tag{20}$$

In shallow-buried explosions, charge energy mainly transforms into the kinetic energy of the ejected rocks; thus, Equation (19) can be simplified into

$$Q = A_1 h_b^3 \left[\frac{1+\omega^2}{2}\right]^2. \tag{21}$$

For hard rocks such as granite, $A_1 = 1.8 - 2.55\,\mathrm{kg/m^3}$ [14].

The shock pressure can be obtained as long as the charge is determined with the help of Equation (21). Considering the fact that the proportion of ground shock energy increases with the buried depth increasing and reaches the maximum when explosions are confined, for confined explosions, the shock pressure decays with distance in the form of [10]

$$\sigma_{\max} = A\left(\frac{r}{Q^{1/3}}\right)^{-n}, \tag{22}$$

where A and n are parameters dependent on rock properties.

For shallow-buried explosions, the stress amplitude of ground shock can be calculated by introducing a coefficient η_Q defined as

$$\eta_Q = \frac{Q_{\mathrm{eff}}}{Q}, \tag{23}$$

where Q_{eff} is the effective charge of the confined explosion which produces the same shock pressure as the shallow-buried explosion does at the same distance.

The stress amplitude of shallow-buried explosions can thus be written as

$$\sigma_{\max} = A\left(\frac{r}{Q_{\mathrm{eff}}^{1/3}}\right)^{-n}, \tag{24}$$

or, more generally,

$$\sigma_{\max} = \eta_\sigma A\left(\frac{r}{Q^{1/3}}\right)^{-n}, \tag{25}$$

where $\eta_\sigma = \eta_Q^{n/3}$ is the coupling coefficient with the meaning of the ratio of stress amplitude of the shallow-buried explosions to that of confined explosions at the same distance. Coefficient η_σ increases with the buried depth increasing and, in general, has the form of

$$\eta_\sigma = \begin{cases} f_*\left(\dfrac{h_b}{Q^{1/3}}\right), & h_b < h_*, \\ 1, & h_b \ge h_*, \end{cases} \tag{26}$$

where $h_* \approx r_0$ is the minimum buried depth of confined explosions. f_* is a monotonic increasing function of the buried depth h_b whose concrete form is closely related to the properties of emplacement rocks.

In practice, a specific form of Equation (25) is used, i.e. [15]

$$\sigma_{\max} = 48.77\eta_\sigma \rho C_p \left(\frac{2.8r}{Q^{1/3}}\right)^{-n}. \tag{27}$$

As long as the stress amplitude is determined, the stress-time relation can be written as [15].

$$\sigma_r(t) = \begin{cases} \sigma_{\max}\dfrac{t}{t_r}, & t \le t_r, \\ \sigma_{\max}\exp\left[-\dfrac{(t-t_r)}{t_a}\right], & t > t_r, \end{cases} \tag{28}$$

where $t_r \approx 0.1t_a$ is the time of stress rising and $t_a = r/C_p$ is the time of stress wave traveling.

4. The Ground Shock of Hypervelocity Impacts

According to the calculation in Section 2, the ground shock of a hypervelocity impact can be regarded as being equivalent to that of a shallow-buried explosion if their crater sizes are the same.

Experiments of projectile impacting show that the characteristics of the impact crater change with the impact velocity [3, 16]. When the impact velocity is relatively low, a deep hole is formed at the center of the crater. The diameter of the hole is slightly larger than that of the projectile. As the impact velocity increases, the hole shortens and eventually vanishes. Meanwhile, the diameter of the crater increases, and the crater shape is becoming similar

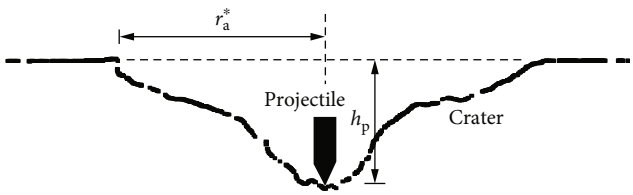

Figure 3: Diagram of the crater of the hypervelocity impact.

to that of the shallow-buried explosion, as is shown in Figure 3.

To equate the ground shock effect of a hypervelocity impact to that of a shallow-buried explosion, an energy equivalent coefficient η is introduced as the ratio of the charge energy to the kinetic energy of the projectile that forms a crater of the same size, i.e.,

$$\eta = \frac{QQ_v}{E_k} = \frac{Q_v A_1 h_p^3 \left[\left(1 + \left(r_a^*/h_p\right)^2\right)/2\right]^2}{0.5Mv_0^2}, \tag{29}$$

where E_k is the kinetic energy of the projectile, M is the projectile mass, v_0 is the impact velocity, and Q_v is the explosion heat of the charge. For TNT, $Q_v \approx 4.18 \times 10^6$ J/kg. In Equation (29), it is assumed that the buried depth of the charge approximately equals the crater depth.

Under hypervelocity impact, the projectile behaves like a jet flow, and the hydrodynamic model is applied to describe the interaction between the projectile and the target [16]:

$$\frac{1}{2}\rho_j\left(v_j - v\right)^2 + Y_j = H_t + \frac{\kappa}{2}\rho_t v^2, \tag{30}$$

where ρ_j and ρ_t are, respectively, the densities of the projectile and the target; Y_j and H_t are, respectively, the dynamic hardness of the projectile and the target; v_j is the velocity of the projectile tail; v is the velocity of the interface between the projectile and the target; and κ is the coefficient of internal friction with the form of

$$\kappa = \begin{cases} \dfrac{1+\nu}{3(1-\nu)}, & v_* \le 1.5, \\ \dfrac{2(1+\nu)/[3(1-\nu)] - 1 + \exp\left(v_{**}\right)}{1 + \exp\left(v_{**}\right)}, & 1.5 < v_*, \end{cases}$$
$$v_{**} = 2\left(v_* - 1.5\right), v_* = \frac{v_0}{c}, \tag{31}$$

where ν is the Poisson's ratio of the target and $c = \left(2H_t/\rho_t\right)^{1/2}$ is the characteristic velocity of the target.

It can be deduced from Equation (31) that $\kappa \longrightarrow 1$ as $v_0 \longrightarrow \infty$, indicating that the target behaves hydrodynamically when the impact velocity is extremely high.

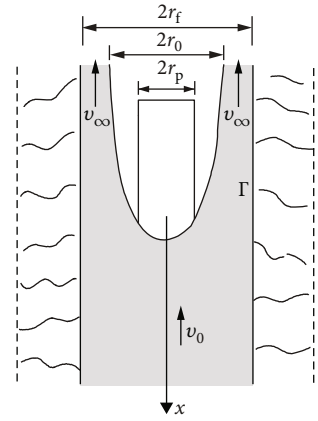

Figure 4: Diagram of the calculation model of crater size.

It follows from Equation (30) that the penetration depth, i.e., the crater depth, is

$$\frac{h_p}{L} = \frac{1 - \sqrt{1 - \left(1 - \left(\kappa/\lambda_p^2\right)\right)(1 - \varpi)}}{\sqrt{1 - \left(1 - \left(\kappa/\lambda_p^2\right)\right)(1 - \varpi)} - \left(\kappa/\lambda_p^2\right)}, \tag{32}$$

where L is the initial length of the projectile, $\lambda_p = \left(\rho_j/\rho_t\right)^{1/2}$, and $\varpi = \left(2(H_t - Y_j)\right)/(\rho_j v_0^2)$. If $v_0 \longrightarrow \infty$, $\varpi \longrightarrow 0$, then

$$\frac{h_p}{L} \longrightarrow \lambda_p, \tag{33}$$

thus $L\lambda_p$ is the limit depth of the crater.

The crater radius can be derived from a jet flow model [17–19]. As is shown in Figure 4, a rigid body with a radius r_p is moving downward in a brittle medium with the velocity v_0. The medium in the fracture region behaves like an ideal compressible liquid of the same density as the initial medium. The internal boundary of the radial-crack region Γ is assumed to be rigid. Then the problem of projectile penetration transforms into the problem of a fluid flowing past an obstruction in a pipeline with a rigid boundary [17].

The Bernoulli equation and continuity equation in the fracture region are

$$\frac{\kappa}{2}\rho_t v_0^2 + H_t = \frac{\kappa}{2}\rho_t v_\infty^2,$$
$$\vartheta_0\left(r_f^2 - r_p^2\right)v_\infty = r_f^2 v_0, \tag{34}$$

where v_∞ is the velocity at infinity distance behind the obstruction and $\vartheta_0 = \left(r_f^2 - r_0^2\right)/\left(r_f^2 - r_p^2\right)$ is the contraction coefficient of the jet.

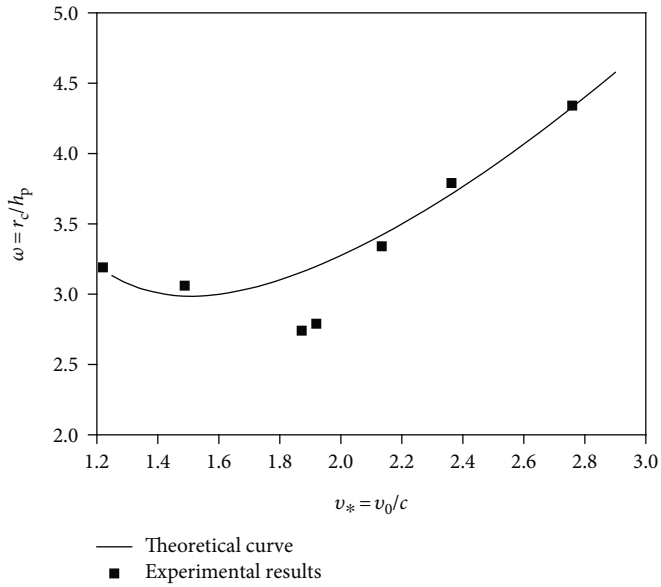

Figure 5: Experimental and theoretical parameter ω vs. scale velocity v_*.

It follows from Equation (34) that

$$r_f = r_p\sqrt{\frac{\vartheta_0\delta}{\vartheta_0\delta - 1}},$$
$$\delta = \sqrt{1 + \frac{1}{\kappa}\frac{1}{v_*^2}}. \tag{35}$$

The theoretical value of ϑ_0 is given by Gurevich [19]:

$$\vartheta_0 = \frac{\varsigma^\chi}{1 - (\varsigma^\chi sin\pi\chi/\pi)\int_0^1[(1/(\xi+\varsigma)) + (1/(\xi+1/\varsigma)) - (2/(\xi+1))]\left(d\xi/\xi^\chi\right)}, \tag{36}$$

where $\chi = \alpha/\pi$, α is the half-angle at the apex of the projectile ($0 < \alpha \le 2\pi$), and $\varsigma^\chi = v_0/v_\infty = (v_*)/(1+v_*^2)^{-1/2}$.

Voitishek and Slepyan [18] further obtain the relation between the radiuses of the radial-crack region and the fracture region:

$$\frac{r_c}{r_f} = \left[\frac{\pi(\phi_* + 0.5)^2}{n_c(1-\phi_*)^2}\right]^{1/3}\left(\frac{H_t^2 r_f}{\gamma_s E}\right)^{1/3}, \tag{37}$$

where γ_s is the effective surface energy, n_c is the number of growing cracks and is assumed to be invariable, E is Young's modulus of the target, and $\phi_* \approx 0.187$ is a constant.

Set $\nu = 1/3$, then $\gamma_s E = \pi K_c^2(1-\nu^2)/2 \approx 1.5K_c^2$, where K_c is the fracture toughness of the target. Besides, $n_c = 6\pi$ is assumed [18], and $\Delta = K_c^2/H_t^2$ is the extent of the plastic zone at the apex of the crack, and then Equation (37) can be simplified into

$$\frac{r_c}{r_f} \approx 0.43\left(\frac{r_f}{\Delta}\right)^{1/3}. \tag{38}$$

Substituting Equations (32) and (38) into Equation (29) produces the analytical solution of coefficient η. The result, however, is quite complicated. Thus, the empirical formula is suggested in practice for convenience.

Since the size of the impact crater has been determined, the parameters of the equivalent shallow-buried explosion are

$$Q = \frac{\eta E_k}{Q_v},$$
$$h_b = h_p. \tag{39}$$

Then the ground shock of hypervelocity impact can be obtained by substituting Equation (39) into Equations (26)–(28).

5. Comparison with Experimental Results

5.1. The Energy Equivalent Coefficient η. Li et al. [16] and Wang et al. [20] conducted hypervelocity impact experiments with metal projectiles and granite targets. The projectile head is of oval shape with the CRH value of 3.0. The length of the projectile $L = 36$ mm, the radius $r_p = 3.6$ mm, the mass $M = 9.67$ g, and the density $\rho_j = 7850\,\mathrm{kg/m^3}$. For targets, the density $\rho_t = 2670\,\mathrm{kg/m^3}$, the longitudinal wave $C_p = 4200$ m/s, the compressive strength $\sigma_c = 150$ MPa, the shear strength $\sigma_s = 50$ MPa, the shear modulus $\mu = 27$ GPa, the fracture toughness $K_c = 2.7\,\mathrm{MPa \cdot m^{1/2}}$, and the dynamic hardness $H_t = 3$ GPa.

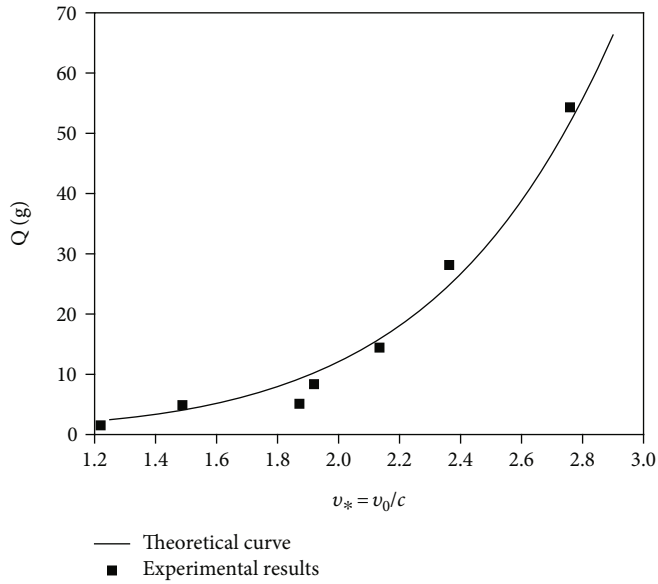

Figure 6: Experimental and theoretical equivalent charge Q vs. scale velocity v_*.

The projectiles were launched at velocities between 1800 and 4200 m/s. The depths and radiuses of craters were measured after experiments; besides, their theoretical values are calculated with Equations (32) and (38), respectively. As a measure of crater shape, parameter ω at different scale velocities is shown in Figure 5. The charge Q of equivalent shallow-buried explosions and the energy equivalent coefficient η are calculated on the basis of experimental and theoretical crater sizes, respectively. The results are separately depicted in Figures 6 and 7.

The change of ω with the velocity reflects the characteristics of craters at different impact velocities. As is shown in Figure 5, ω decreases as v_* increases when $v_* < 1.5$, corresponding to the conditions of rigid penetration and quasi-fluid penetration [16] where crater depths develop faster than crater radiuses do. When $v_* > 1.5$, however, ω increases with v_* increasing, indicating that crater radiuses develop faster than crater depths do. The region $v_* < 1.5$ is not taken into account in this paper because the penetration effect, rather than the ground shock effect, predominates in this region. Besides, the crater shape in this region is not similar to that of shallow-buried explosions.

Figure 6 shows that the equivalent charge Q increases as the impact velocity increases. It is only natural that the energy of ground shock induced by impacts is larger for projectiles with higher kinetic energy.

Figure 7 illustrates the change of η with v_*. According to the definition of η, the region $\eta < 1$ corresponds to the case where more kinetic energy than explosion energy is needed to produce the same ground shock energy. In other words, shallow-buried explosions have higher energy conversion efficiency in terms of ground shock than high-velocity impacts do. For the region $\eta > 1$, however, the reverse applies. The critical value $\eta = 1$ corresponds to the special case where hypervelocity impacts and shallow-buried explosions are completely equivalent in terms of energy.

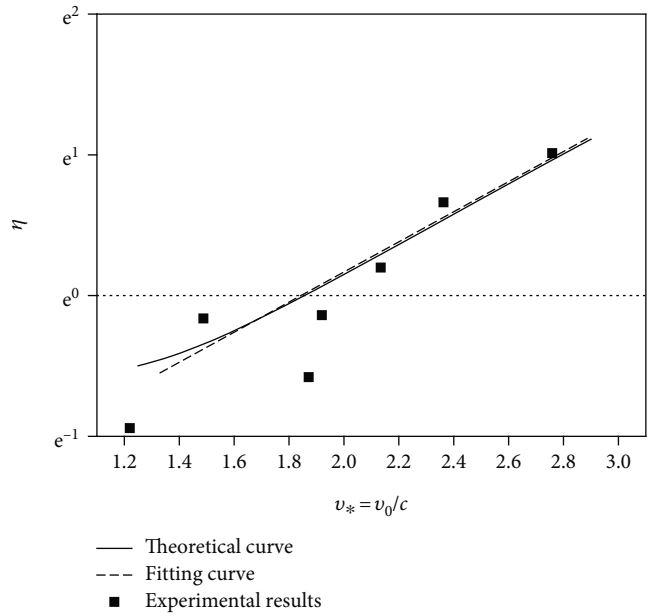

Figure 7: Experimental and theoretical coefficient η vs. scale velocity v_*.

Considering the fact that hypervelocity projectiles compress the ground in one direction and that explosions release energy in all directions, hypervelocity impacts are supposed to transform a larger proportion of energy into ground shock energy than explosions do. In this connection, it can be inferred that for hypervelocity impacts, the penetration effect still predominates when $\eta < 1$. Thus the case $\eta < 1$ is also not taken into account in this paper for the equivalent calculation.

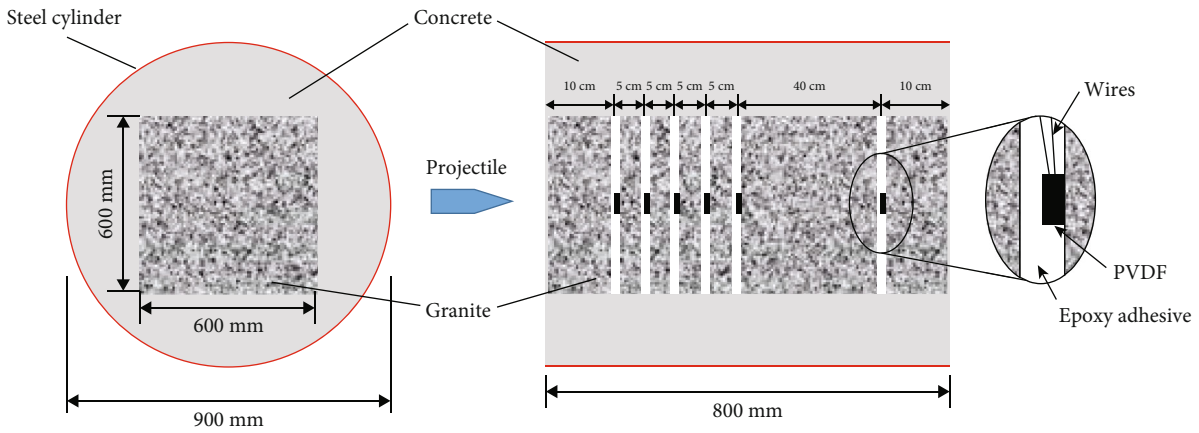

Figure 8: Diagram of targets.

As is shown in Figure 7, $\eta > 1$ when $v_* > 1.88$, and then the simplified expression of η can be written as

$$\eta = e^{v_* - 1.88}, \tag{40}$$

or more generally,

$$\eta = k_a e^{v_*}, \tag{41}$$

where k_a is the coefficient dependent on the properties of the projectile and target.

5.2. Verification for the Equivalent Calculation. In order to measure the stress of ground shock induced by projectile impacting, the granite targets were made of blocks with different thicknesses, and PVDF piezoelectric gauges were placed between adjacent blocks. The structure of targets and the layout of gauges are shown in Figure 8.

Figure 9 shows the time history curves of stresses at different distances when $v_0 = 3558$ m/s. The maximum stress at the first layer is approximately 401 MPa. Given that the Hugoniot elastic limit of granite exceeds 3 GPa [21], it can be inferred that the measurement points are in the elastic region. Fitting the maximum stresses with exponential law produces the curve of stress attenuating with distance, as shown in Figure 10. The parameter n in Equation (25) is determined as 1.4.

The scale velocity corresponds to 3558 m/s is $v_* = 2.37$. Substituting this value into Equation (40) gives $\eta = 1.63$, indicating that the energy of the equivalent shallow-buried explosion equals 1.63 times the kinetic energy of the projectile. The equivalent charge Q can be calculated with Equation (39). In this case, $Q = 2.39 \times 10^{-2}$ kg. Besides, $n = 1.4$, $t_r \approx 0.1 t_a$, and $\eta_c = 0.7$. Substituting these parameters into Equations (27) and (28) produces the theoretical ground shock of the equivalent shallow-buried explosion. The time history curves of stresses are shown in Figure 11.

In general, the theoretical stresses in Figure 11 agree well with the experimental values in Figure 9. However, secondary stress peaks are detected after the main peaks of curves

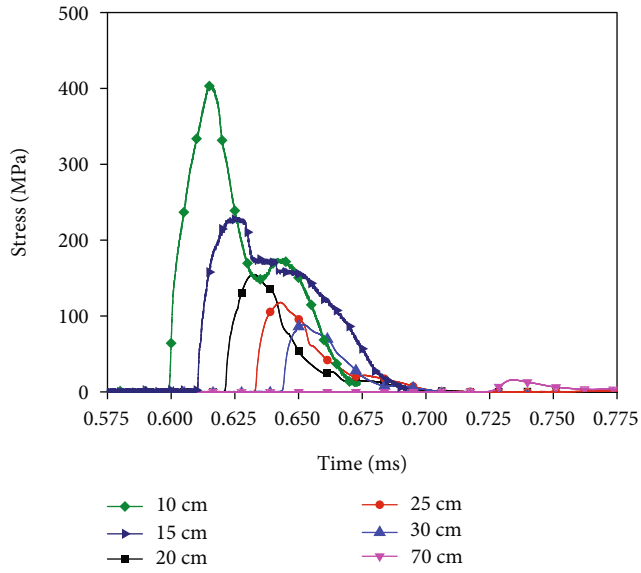

Figure 9: Time history curves of stresses.

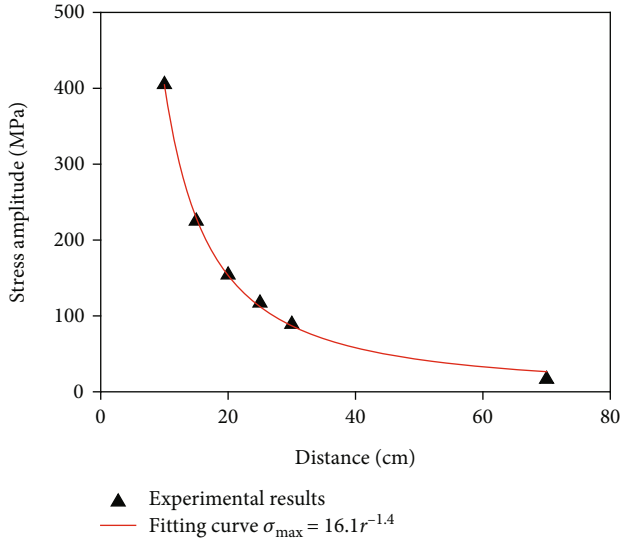

Figure 10: Attenuation of stresses with distance.

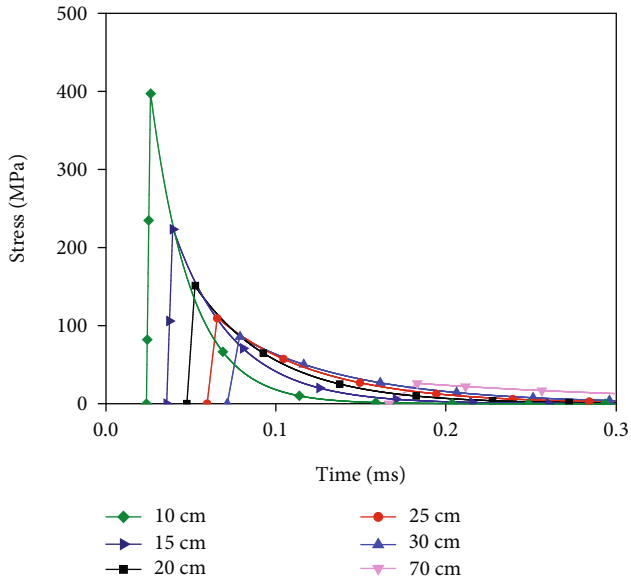

Figure 11: Time history curves of stresses of the equivalent shallow-buried explosion.

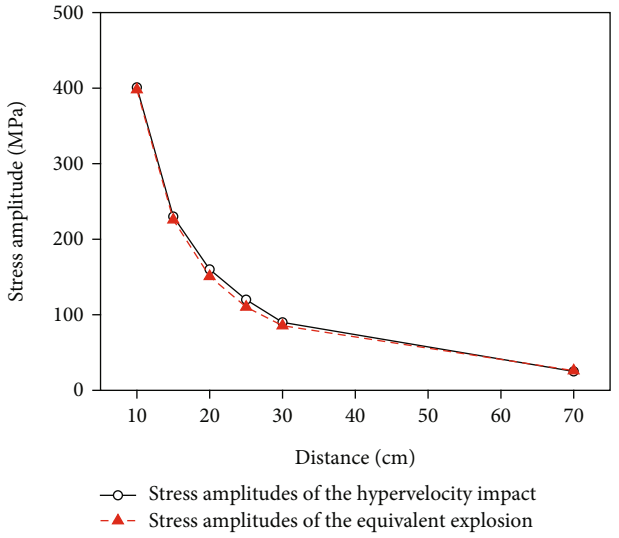

Figure 12: Stress attenuation curves of the hypervelocity impact and the equivalent explosion.

in Figure 9, and the stress attenuation is weaker for experimental curves than for theoretical curves. These may be due to the reflection effect on the interlayers between adjacent granite blocks.

Figure 12 shows the stress attenuation curves of the hypervelocity impact and the equivalent explosion. As is shown in the figure, the experimental and theoretical stress amplitudes at the same distance agree well with each other, especially for $r = 10$ cm, 15 cm, and 70 cm, where two values are nearly the same. In this connection, the effectiveness of the equivalent method proposed in this paper is proved.

6. Conclusions

(a) In the impact and explosion events, the shock energy radiating from a certain region underground is proportional to the mass of the materials in the region. The coefficient is determined by the properties of the materials

(b) The dimensionless factor k can be used to define the boundaries of different regions. Each boundary of the regions (crater, fracture region, and radial-crack region) corresponds to a constant k dependent upon the properties of the materials. Based on the invariability of k, the equivalent method for estimating impact-induced ground shock is proposed: The ground shock of an impact is regarded as being equivalent to that of an explosion if their crater sizes are the same

(c) Comparison is carried out between the calculated and experimental ground shock. The fitted energy equivalent coefficient η changes exponentially with the impact velocity. The calculated stress-time curves and the stress attenuation curve agree well with the experimental curves

Data Availability

The data used to support the findings of this study are available from the corresponding author upon request.

Conflicts of Interest

The authors declare that they have no known competing financial interests or personal relationships that could have appeared to influence the work reported in this paper.

Acknowledgments

This research was financed and fully supported by the National Natural Science Foundation of China (Grant: 51679249, 11772355, 42002266, and 12072371) and the Postgraduate Research & Practice Innovation Program of Jiangsu Province (Grant: KYCX20_0312), which are greatly appreciated by the authors.

References

[1] S. Nakazawa, "Experimental investigation of shock wave attenuation in basalt," *Icarus*, vol. 156, no. 2, pp. 539–550, 2002.

[2] K. Shirai, M. Kato, N. K. Mitani, and M. Arakawa, "Laboratory impact experiments and numerical simulations on shock pressure attenuation in water ice," *Journal of Geophysical Research*, vol. 113, no. E11, 2008.

[3] M. Wang, Y. Qiu, J. Li, H. Li, and Z. Zhao, "Theoretical and experimental study on rock penetration and ground impact effects of hypervelocity long rod projectiles," *Chinese Journal of Rock Mechanics and Engineering*, vol. 37, pp. 564–572, 2018.

[4] H. J. Melosh, "Impact cratering mechanics: relationship between the shock wave and excavation flow," *Icarus*, vol. 62, no. 2, pp. 339–343, 1985.

[5] C. Mok, "Effects of solid strength on the propagation and attenuation of spherical and plane shock waves," *Journal of Applied Physics*, vol. 39, no. 4, pp. 2072–2081, 1968.

[6] M. R. Dence, A. Bischoff, and V. Buchwald, "Terrestrial impact structures-principal characteristics and energy considerations," in *Impact and Explosion Cratering: Planetary and Terrestrial Implications: Proceedings of the Symposium on Planetary Cratering Mechanics*, pp. 247–275, Flagstaff, Arizona, 1977.

[7] T. G. Sharp and P. S. de Carli, "Shock Effects in Meteorites," *Meteorites and the early solar system II*, vol. 943, p. 653, 2006.

[8] X. Wang, J. Li, X. Zhao, and Y. Liang, "Propagation characteristics and prediction of blast-induced vibration on closely spaced rock tunnels," *Tunnelling and Underground Space Technology*, vol. 123, p. 104416, 2022.

[9] V. Rodinov, V. Adushkin, V. Kostuchenko, V. Nikolaevskii, A. Rosashov, and V. Tsvetkov, *Mechanical Effect of an Underground Explosion*, Nedra, Moscow, 1971.

[10] V. V. Adushkin and A. Spivak, *Underground explosions*, Washington, DC: U. S. Department of State, 2015.

[11] N. A. Haskell, "Analytic approximation for the elastic radiation from a contained underground explosion," *Journal of Geophysical Research*, vol. 72, no. 10, pp. 2583–2587, 1967.

[12] N. I. Shishkin, "Seismic efficiency of a contact explosion and a high-velocity impact," *Journal of Applied Mechanics and Technical Physics*, vol. 48, no. 2, pp. 145–152, 2007.

[13] M. Wang and J. Li, "Nonlinear mechanics problems in rock explosion and shock. Part III: the calculation principle of engineering seismic effects induced by underground nuclear explosion and its application," *Chinese Journal of Rock Mechanics and Engineering*, vol. 38, pp. 695–707, 2019.

[14] J. Henrych, *The Dynamics of Explosion and Its Use*, Elsevier, Amsterdam, 1979.

[15] TM-855-1, *Fundamentals of Protective Design for Conventional Weapons*, U.S. Army Engineer Waterways Experiment Station, Vicksburg, Mississippi, 1986.

[16] J. Li, M. Wang, Y. Cheng, and Y. Qiu, "Analytical model of hypervelocity penetration into rock," *International Journal of Impact Engineering*, vol. 122, pp. 384–394, 2018.

[17] L. I. Slepyan, "Calculation of the size of the crater formed by a high-speed impact," *Soviet Mining Science*, vol. 14, no. 5, pp. 465–471, 1978.

[18] Y. V. Voitishek and L. I. Slepyan, "Hydrodynamic model of the puncture of a brittle plate," *Soviet Mining Science*, vol. 21, no. 3, pp. 231–235, 1985.

[19] M. I. Gurevich, *The Theory of Jets in an Ideal Fluid*, Pergamon Press Ltd, London, 1966.

[20] M. Wang, S. Yue, H. Li, Y. Qiu, and J. Li, "Equivalent calculation study on ground shock effects of hypervelocity projectile striking on rock," *Chinese Journal of Rock Mechanics and Engineering*, vol. 37, pp. 2655–2663, 2018.

[21] J. T. Rosenberg, *Dynamic Shear Strength of Shock-Loaded Granite and Polycrystalline Quartz*, Menlo Park, California, Stanford Research Institute, 1971.